Optimizing Encoding Strategies for 4D Flow MRI of Mean and Turbulent Flow: Supplementary Material

Pietro Dirix*, Stefano Buoso & Sebastian Kozerke

Institute for Biomedical Engineering, University and ETH Zurich, Zurich, Switzerland

Supplementary Methods

Details on the computation of the Reynolds stress tensor

For a given time t in the cardiac cycle, the total Reynolds stress tensor ($\boldsymbol{R^{tot}} \in \mathbb{R}^{3\times 3}$) is defined as:

$$\boldsymbol{R^{tot}} = \frac{\rho}{N}\sum_{n=1}^{N}(\boldsymbol{u_n} - \overline{\boldsymbol{u}})\,(\boldsymbol{u_n} - \overline{\boldsymbol{u}})^{\mathrm{T}} + \frac{\rho}{N}\sum_{n=1}^{N}\boldsymbol{R_{sgm}} \tag{1}$$

where, $\overline{\blacksquare}$ is the averaging operator, $\boldsymbol{u} = (\boldsymbol{u_1}, \boldsymbol{u_2}, \dots, \boldsymbol{u_N}) \in \mathbb{R}^{3\times N}$ is the velocity vector including sampled velocities over N cardiac cycles, and $\boldsymbol{R_{sgm}} \in \mathbb{R}^{3\times 3}$ is the modelled sub-grid Reynolds stress tensor. Additionally, we introduce two methods for temporal averaging of the total Reynolds stress tensor $\boldsymbol{R_M^{tot}} \in \mathbb{R}^{3\times 3\times M}$ (and its corresponding vector field $\boldsymbol{U} \in \mathbb{R}^{3\times M}$), where M is the number of temporal frames to average:

$$\overline{\boldsymbol{R}}_a = \frac{1}{M}\sum_{m=1}^{M}\boldsymbol{R_m^{tot}} \tag{2}$$

$$\overline{\boldsymbol{R}}_b = \frac{1}{M}\sum_{m=1}^{M}\boldsymbol{R_m^{tot}} + \frac{\rho}{M}\sum_{m=1}^{M}\boldsymbol{U}_m\,\boldsymbol{U}_m{}^{\boldsymbol{T}} - \rho\overline{\boldsymbol{U}}\overline{\boldsymbol{U}}^{\boldsymbol{T}} \tag{3}$$

where $\boldsymbol{R_m^{tot}}$ corresponds to the m^{th} temporal frame of $\boldsymbol{R_M^{tot}}$, $\overline{\boldsymbol{R}}_a$ is the average Reynolds stress tensor (RST) using the definition of the arithmetic mean and $\overline{\boldsymbol{R}}_b$ is a modified averaged RST that accounts for contributions of the velocities to the RST during averaging[1]. In the main manuscript, all mentions to RST refer to $\overline{\boldsymbol{R}}_b$, MRI does not measure arithmetic means of fluctuations when combining measurements with successive TRs.

Details on the MRI signal model

Similarly to our previous work, N cardiac cycles were used to generate mean velocity $\overline{\boldsymbol{u}}$ and total Reynolds stress tensor $\boldsymbol{R^{tot}}$ for each time t in the cardiac cycle. These quantities were then downsampled to cycle averaged velocity $\overline{\boldsymbol{u}}_{\boldsymbol{\Delta}}$ and RST $\boldsymbol{R_\Delta}$ at MRI resolution by first projecting them onto a uniform grid with isotropic voxel size $L = 0.65mm$ and then downsampling them to a uniform grid with isotropic voxel size $\Delta_L = 2.5mm$:

$$\overline{\boldsymbol{u}}_{\boldsymbol{\Delta}} = \boldsymbol{\mathcal{F}}^{-\mathbf{1}}(\boldsymbol{\mathcal{F}}(\overline{\boldsymbol{u}}) \circ \omega) \tag{4}$$

$$\boldsymbol{R}_{\boldsymbol{\Delta}} = \boldsymbol{\mathcal{F}}^{-\mathbf{1}}(\boldsymbol{\mathcal{F}}(\boldsymbol{R}^{tot}) \circ \omega) + \rho \boldsymbol{\mathcal{F}}^{-\mathbf{1}}\left(\boldsymbol{\mathcal{F}}\left(\overline{\boldsymbol{u}}\overline{\boldsymbol{u}}^{\boldsymbol{T}}\right) \circ \omega\right) - \rho \overline{\boldsymbol{u}}_{\boldsymbol{\Delta}} \overline{\boldsymbol{u}}_{\boldsymbol{\Delta}}^{\boldsymbol{T}} \tag{5}$$

where $\boldsymbol{\mathcal{F}}$ is the Fourier operator, $\circ$ is the apodization operator and ω is a truncated 3D Gaussian modular transfer function (MTF) with standard deviation $\sigma_G = \sqrt{8 \ln 2}\, L/\Delta_{\mathrm{L}}$. The truncation window is a box with width $w \propto L/\Delta_{\mathrm{L}}$, such that the Gaussian MTF is truncated at an amplitude of 0.5 along each principal Cartesian direction. This allows us to generate ideal synthetic MRI data as in[1]. We expanded on this approach to include downsampling of instantaneous velocity quantities, such that for each cardiac cycle n:

$$\boldsymbol{u}_{\mathbf{n},\boldsymbol{\Delta}} = \boldsymbol{\mathcal{F}}^{-\mathbf{1}}(\boldsymbol{\mathcal{F}}(\boldsymbol{u}_{\boldsymbol{n}}) \circ \omega) \tag{6}$$

$$\boldsymbol{R}_{\mathbf{n},\boldsymbol{\Delta}} = \boldsymbol{\mathcal{F}}^{-\mathbf{1}}\left(\boldsymbol{\mathcal{F}}\left(\boldsymbol{R}_{\boldsymbol{sgm}}\right) \circ \omega\right) + \rho \boldsymbol{\mathcal{F}}^{-\mathbf{1}}\left(\boldsymbol{\mathcal{F}}\left(\boldsymbol{u}_{\boldsymbol{n}} \boldsymbol{u}_{\boldsymbol{n}}^{\boldsymbol{T}}\right) \circ \omega\right) - \rho \boldsymbol{u}_{\mathbf{n},\boldsymbol{\Delta}} \boldsymbol{u}_{\mathbf{n},\boldsymbol{\Delta}}^{\boldsymbol{T}} \tag{7}$$

where $\boldsymbol{u}_{\mathbf{n},\boldsymbol{\Delta}}$ and $\boldsymbol{R}_{\mathbf{n},\boldsymbol{\Delta}}$ are the instantaneous velocity and RST at a given cardiac cycle at MRI resolution.

The MR signal $\boldsymbol{S}_{\boldsymbol{n}}$ for each cardiac cycle n can be finally written as:

$$\begin{gathered} \boldsymbol{S}_{\boldsymbol{n}}\left(\boldsymbol{k}_{\boldsymbol{v},\boldsymbol{i}}\right) = S_0 e^{-\frac{\rho^{-1} \boldsymbol{k}_{\boldsymbol{v},\boldsymbol{i}} \boldsymbol{R}_{\boldsymbol{n},\boldsymbol{\Delta}} \boldsymbol{k}_{\boldsymbol{v},\boldsymbol{i}}{}^{\mathrm{T}}}{2}} e^{-j \boldsymbol{k}_{\boldsymbol{v},\boldsymbol{i}} \boldsymbol{u}_{\boldsymbol{n},\boldsymbol{\Delta}}} + \eta \\ \boldsymbol{S}_{\boldsymbol{n}} \in \mathbb{C}^{k_x \times k_y \times k_z} \end{gathered} \tag{8}$$

where $\boldsymbol{k}_{\boldsymbol{v},\boldsymbol{i}} = k_{v,i} \vec{\boldsymbol{e}}_i = \left[k_{vx}, k_{vy}, k_{vz}\right]_i \in \mathbb{R}^{1\times 3}$ represents flow sensitivity along the i^{th} direction with encoding velocity frequency $k_{v,i} = \pi/[V_{enc}]_i$, proportional to a directional encoding velocity V_{enc}. $\eta \propto \mathrm{SNR}$ is complex Gaussian noise with zero mean and standard deviation $\sigma_\eta = |\bar{S}_{ROI}| \cdot (\mathrm{SNR})^{-1}$ with $\bar{S}_{ROI}$ being the mean noise-free signal in the simulated aorta. In this work, SNR was set to 20. S_0 is the normalized reference signal without velocity encoding that in this work was proportional to the cubic root of normalized velocity and bounded between 0.5 and 1. Signal based on cycle averaged quantities can be obtained by replacing $\boldsymbol{R}_{\boldsymbol{n},\boldsymbol{\Delta}}$ and $\boldsymbol{u}_{\boldsymbol{n},\boldsymbol{\Delta}}$ by $\boldsymbol{R}_{\boldsymbol{\Delta}}$ and $\boldsymbol{u}_{\boldsymbol{\Delta}}$, respectively.

Details on the generation of the k-space sampling pool

Fully sampled complex-valued MRI data was used as input for retrospectively simulating undersampled k-space. To represent the process, we defined the global pool of available instantaneous k-space data $\boldsymbol{S}^{\boldsymbol{k}}$ as:

$$\begin{gathered} \boldsymbol{S}^{\boldsymbol{k}} = \boldsymbol{\mathcal{F}}(\boldsymbol{S}_{\boldsymbol{t}} * \boldsymbol{C}) \\ \boldsymbol{S}_{\boldsymbol{t}} \in \mathbb{C}^{k_x \times k_y \times k_z \times N_{cp} \times N_{hb} \times N_v} \\ \boldsymbol{C} \in \mathbb{C}^{k_x \times k_y \times k_z \times N_{coil}} \\ \boldsymbol{S}^{\boldsymbol{k}} \in \mathbb{C}^{k_x \times k_y \times k_z \times N_{cp} \times N_{hb} \times N_v \times N_{coil}} \end{gathered} \tag{9}$$

where $k_x \times k_y \times k_z$ are the dimensions of the imaging volume, N_v is the number of encoding directions, $N_{coil} = 8$ is the number of coils, $\boldsymbol{C}$ are the coil sensitivity maps and $\boldsymbol{S}_{\boldsymbol{t}}$ are the instantaneous MR images obtained from generating $\boldsymbol{S_n}$ for all CFD cardiac phases, CFD cardiac cycles and encoding directions.

The final prospectively undersampled k-space data $\boldsymbol{S}_{R_u}^{k}$ defined by the undersampling trajectory can be described by:

$$\begin{gathered}\boldsymbol{S}_{R_u}^{k}\left(k_x,:,k_z,n_{cp,MRI},n_v,:\right)=\boldsymbol{\Omega}(k_x,:,k_z,n_{cp,MRI},n_v)\cdot \\ \boldsymbol{S^k}\left(k_x,:,k_z,\boldsymbol{f}\left(n_{cp,MRI}\right),U(0,N_{hb}),n_v,:\right) \\ \boldsymbol{\Omega}\in\mathbb{C}^{k_x\times k_y\times k_z\times N_{cp,MRI}} \\ \boldsymbol{S}_{R_u}^{k}\in\mathbb{C}^{k_x\times k_y\times k_z\times N_{cp,MRI}\times N_v\times N_{coil}}\end{gathered} \tag{10}$$

where the operator $\boldsymbol{f}(\blacksquare)$ bins the higher number of simulated cardiac phases (80) in $\boldsymbol{S^k}$ to $N_{cp,MRI}$ cardiac phases (19). To mimic acquisition during different cardiac cycles, n_{hb} is randomly sampled for each individual spoke using a continuous uniform distribution $U(0,N_{hb})$. The ":" indicates that all points along that direction are filled simultaneously (frequency encoding and coil dimensions).

Details on Reynolds stress tensor reconstruction

The RST can be determined by encoding along six non-collinear directions ($N_v=6$) and solving a system of linear equations. For six measurements along six different velocity encoding directions $\{i\mid i\in\mathbb{Z},1\le i\le 6\}$, $\sigma_{k_v,i}$ was obtained from the ratio between $S^*(\boldsymbol{k_{v,i}})$ and $S^*(0)$ as:

$$\sigma_{k_v,i}^2=\frac{2}{\left|\boldsymbol{k_{v,i}}\right|^2}\ln\frac{|S^*(0)|}{\left|S^*(\boldsymbol{k_{v,i}})\right|} \tag{11}$$

The elements of the RST can be calculated voxel-wise using the pseudoinverse:

$$\boldsymbol{r}^*=\left(\boldsymbol{H}^{\mathrm{T}}\boldsymbol{H}\right)^{-1}\boldsymbol{H}^{\mathrm{T}}\boldsymbol{\sigma}_{\boldsymbol{k_v}}^{\boldsymbol{2}} \tag{12}$$

where $\boldsymbol{\sigma}_{\boldsymbol{k_v}}\in\mathbb{R}^{6\times 1}$ is the intra-voxel standard deviation (IVSD) vector, $\boldsymbol{H_i}\left(\boldsymbol{k_{v,i}},\rho\right)$ is the i^{th} row of $\boldsymbol{H}(\boldsymbol{k_v},\rho)\in\mathbb{R}^{6\times 6}$**,** a transformation matrix that depends on $\boldsymbol{k_v}\in\mathbb{R}^{6\times 3}$. The symmetric RST vector $\boldsymbol{r}^*\in\mathbb{R}^{6\times 1}$ can be recast into its tensor representation $\boldsymbol{R}^*\in\mathbb{R}^{3\times 3}$. The elements along the diagonal represent velocity fluctuation variances while the off-diagonal elements represent covariances.

Details on velocity reconstruction

Redundant encoding schemes provide additional information for estimation of mean velocities. Similarly to the RST, a pseudo-inverse approach can be used to combine 6 independent velocity measurements into $\boldsymbol{u}^*\in\mathbb{R}^{3\times 1}$, the Cartesian velocity vector.

Details on Bayesian reconstruction

For multi-point acquisitions, where the same encoding direction is acquired with different V_{enc} values, each acquisition was combined using Bayesian multipoint unfolding[2] and processed to obtain $\boldsymbol{u}^*$, $\boldsymbol{R}^*$, TKE and KE when 6 encoding directions were acquired, or $\boldsymbol{u}^*$, TKE and KE for the case with 3 directions.

Details on phase unwrapping

For all acquisitions with $V_{enc} \leq 1ms^{-1}$, the phase was ideally unwrapped using the underlying ground truth. This approach allows to evaluate the maximum potential of low-V_{enc} acquisitions at the condition of being able to perfectly unwrap flow data. However, in practical applications and without access to high-V_{enc} data, wrapped phase fields must be algorithmically unwrapped[3]. Although the unwrapping process might be trivial for well-behaved smooth flow (where the phase difference between adjacent spatial and temporal voxels lies between –π and π), phase maps from 4D flow MRI data suffer from limited spatial and temporal resolutions and are typically corrupted by noise and undersampling artifacts, affecting the efficacy of unwrapping algorithms. The process of phase unwrapping can be presented as:

$$\psi = \mathcal{U}(\phi) = \phi + 2n\pi \tag{13}$$

where ϕ is the wrapped phase, n is an integer representing the number of wraps, U is an unwrapping function and ψ is the unwrapped phase. Unwrapping methods attempt to find the variable n. We tested three unwrapping algorithms on our data: a Laplacian based method[3], a method based on sorting by realibility following a noncontinous path (NPRS)[4] and a graph-cut based maximum flow method (PUMA)[5]. The Laplacian and PUMA approaches were implemented in 4D, while the NPRS approach was only implemented in 3D. The unwrapping code is available at https://gitlab.ethz.ch/ibt-cmr-public/4dflow-unwrap.

Supplementary results

Reconstructed data using optimally tuned reconstruction parameters

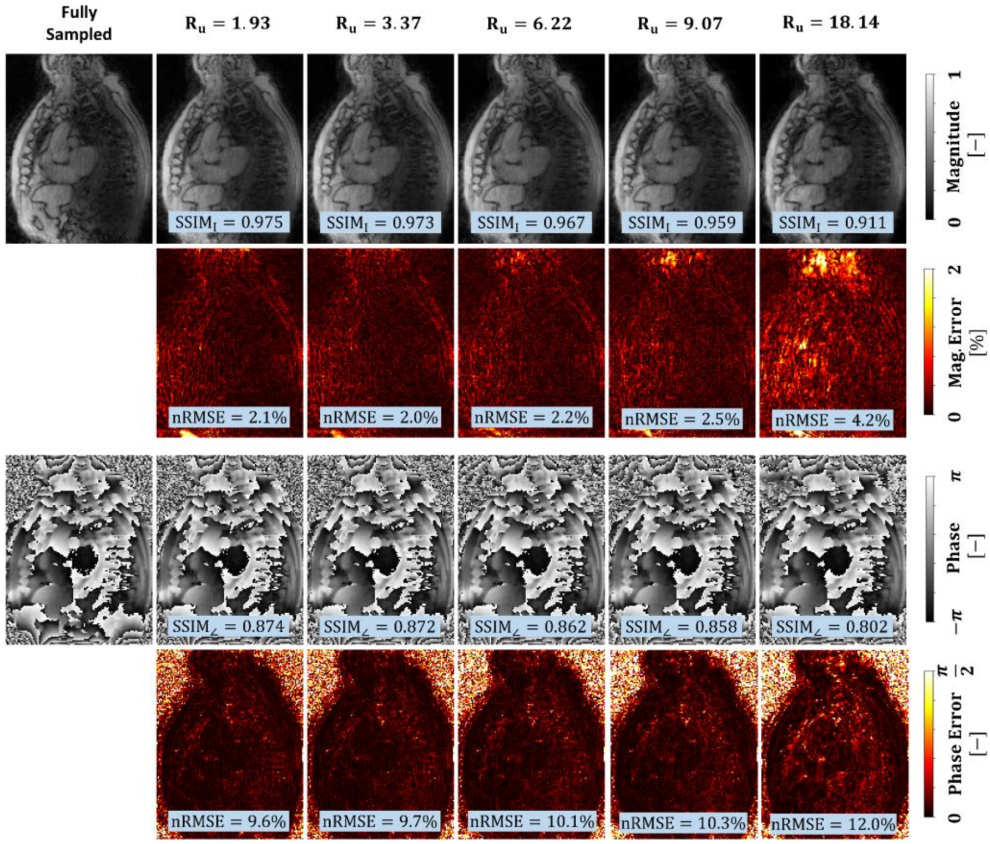

Figure S1: Reconstructed images at peak systole for various undersampling factors R_u. From top to bottom: image magnitude ($|\boldsymbol{I}|$), relative magnitude error compared to the fully sampled case, image phase ($\angle\boldsymbol{I}$) and absolute phase error compared to the fully sampled case.

Impact of encoding strategy

	$\boldsymbol{U_{max}}$ $[\boldsymbol{ms^{-1}}]$	$\boldsymbol{iKE}$ $[\boldsymbol{mJ}]$	$\boldsymbol{SSIM_U}$	$\boldsymbol{VNR}$	$\vec{\boldsymbol{U}}_{\boldsymbol{rmse}}$	$\vec{\boldsymbol{\theta}}_{\boldsymbol{err}}$	$\boldsymbol{\nabla \cdot U}$
CFD	2.17	60.297	-	-	-	-	-
Reference $(snr = \infty)$	2.064	51.628	-	-	-	-	2.584
19p Ideal $(snr = 20)$	2.065 ± 0.006	51.654 ± 0.021	$0.999 \pm 1e^{-4}$	72.036	2.128 ± 0.015	0.104 ± 0.006	3.837 ± 0.033
19p Fully Sampled	2.040 ± 0.004	56.267 ± 0.060	0.944 ± 0.001	66.493	15.037 ± 0.057	3.426 ± 0.028	5.476 ± 0.091
4p (0.5)	2.065 ± 0.004	58.703 ± 0.101	0.933 ± 0.001	65.591	17.260 ± 0.107	3.844 ± 0.053	8.937 ± 0.126
4p (1)	2.013 ± 0.008	56.525 ± 0.102	0.939 ± 0.001	46.328	15.698 ± 0.152	3.707 ± 0.058	6.912 ± 0.095
4p (1)**	2.014 ± 0.009	56.542 ± 0.103	0.939 ± 0.001	46.727	15.698 ± 0.152	3.703 ± 0.057	6.911 ± 0.092
4p (2)	2.000 ± 0.017	53.950 ± 0.083	0.933 ± 0.001	28.229	17.283 ± 0.143	4.271 ± 0.064	10.560 ± 0.138
4p (2)**	1.997 ± 0.016	53.964 ± 0.085	0.933 ± 0.001	28.488	17.284 ± 0.149	4.278 ± 0.063	10.583 ± 0.129
7p (0.5,1)	2.065 ± 0.007	57.861 ± 0.093	0.940 ± 0.001	57.822	15.118 ± 0.094	3.454 ± 0.050	5.773 ± 0.066
7p (0.5,2)	2.070 ± 0.007	57.963 ± 0.119	0.936 ± 0.001	51.829	15.666 ± 0.098	3.579 ± 0.057	6.659 ± 0.072
7p (1,2)	2.004 ± 0.014	54.556 ± 0.081	0.943 ± 0.001	39.331	15.412 ± 0.140	3.677 ± 0.068	6.344 ± 0.071
7p (1,2)**	2.009 ± 0.013	54.654 ± 0.062	0.943 ± 0.001	40.745	15.408 ± 0.141	3.670 ± 0.063	6.304 ± 0.081
7p (0.5)	2.055 ± 0.005	58.010 ± 0.090	0.940 ± 0.001	68.011	16.179 ± 0.082	3.626 ± 0.050	7.668 ± 0.117
7p (1)	1.993 ± 0.011	55.365 ± 0.088	0.942 ± 0.001	49.927	15.298 ± 0.064	3.601 ± 0.046	5.477 ± 0.065
7p (1)**	1.999 ± 0.010	55.456 ± 0.084	0.942 ± 0.001	51.740	15.300 ± 0.067	3.592 ± 0.045	5.462 ± 0.076
7p (2)	1.974 ± 0.016	52.738 ± 0.069	0.937 ± 0.001	30.909	16.305 ± 0.099	3.981 ± 0.064	7.817 ± 0.125
7p (2)**	1.986 ± 0.016	52.953 ± 0.068	0.938 ± 0.001	33.311	16.276 ± 0.102	3.951 ± 0.043	7.711 ± 0.087
13p (0.5,1)	2.031 ± 0.010	62.380 ± 1.118	0.939 ± 0.001	40.627	14.966 ± 0.061	3.398 ± 0.045	5.440 ± 0.076
13p (0.5,2)	2.040 ± 0.010	56.650 ± 0.131	0.933 ± 0.001	50.547	15.486 ± 0.079	3.505 ± 0.046	6.281 ± 0.097
13p (1,2)	1.960 ± 0.018	53.276 ± 0.062	0.939 ± 0.001	39.034	15.268 ± 0.072	3.592 ± 0.064	5.930 ± 0.062
13p (1,2)**	1.965 ± 0.015	53.389 ± 0.059	0.940 ± 0.001	40.791	15.238 ± 0.067	3.585 ± 0.053	5.845 ± 0.062
19p (0.5,1,2)	2.007 ± 0.008	54.357 ± 0.095	0.936 ± 0.001	45.798	15.081 ± 0.093	3.426 ± 0.057	5.609 ± 0.093

*Table S1: Flow metrics depending on the encoding strategy for the cardiac phase corresponding to peak iKE. Rows indicate encoding strategies, "4p (1)" refers to a 4 points encoding scheme with a single V_{enc} of $1ms^{-1}$. Peak velocity (U_{max}), flow rate (Q), integrated kinetic energy (iKE), velocity-to-noise ratio (VNR), and SSIM of velocity ($SSIM_U$) are obtained from 20 repetitions of the same acquisition. Acquistions indicated by ** assume a variable TR depending on V_{enc} (TR = 5, 4.7 and 4.3ms for V_{enc} = 0.5, 1 and 2, respectively).*

	$\boldsymbol{iTKE}$ $[\boldsymbol{mJ}]$	$\boldsymbol{SSIM_{TKE}}$	$\boldsymbol{TNR}$	$\boldsymbol{SSIM_{R_{xy}}}$	$\boldsymbol{SSIM_{R_{xz}}}$	$\boldsymbol{SSIM_{R_{yz}}}$
CFD	3.548	-	-	-	-	-
Reference $(snr = \infty)$	6.947	-	-	-	-	-

19p Ideal ($snr = 20$)	7.028 ± 0.009	$0.972 \pm 1e^{-4}$	7.269	0.802 ± 0.004	0.750 ± 0.005	0.664 ± 0.004
19p Fully Sampled	7.967 ± 0.197	0.637 ± 0.013	6.348	0.296 ± 0.009	0.192 ± 0.010	0.206 ± 0.007
4p (0.5)	5.411 ± 0.022	0.680 ± 0.002	7.073	-	-	-
4p (1)	7.804 ± 0.028	0.649 ± 0.003	4.168	-	-	-
4p (1)**	7.791 ± 0.028	0.650 ± 0.003	4.205	-	-	-
4p (2)	11.334 ± 0.083	0.323 ± 0.003	2.156	-	-	-
4p (2)**	11.314 ± 0.083	0.323 ± 0.003	2.171	-	-	-
7p (0.5,1)	7.736 ± 0.162	0.639 ± 0.027	6.506	-	-	-
7p (0.5,2)	6.965 ± 0.044	0.631 ± 0.006	6.011	-	-	-
7p (1,2)	8.760 ± 0.104	0.616 ± 0.007	3.855	-	-	-
7p (1,2)**	8.684 ± 0.124	0.620 ± 0.008	3.931	-	-	-
7p (0.5)	5.594 ± 0.021	0.666 ± 0.002	6.349	0.270 ± 0.004	0.134 ± 0.005	0.176 ± 0.006
7p (1)	8.186 ± 0.034	0.647 ± 0.003	3.739	0.320 ± 0.005	0.214 ± 0.007	0.159 ± 0.004
7p (1)**	8.115 ± 0.032	0.650 ± 0.003	3.816	0.322 ± 0.005	0.216 ± 0.006	0.164 ± 0.004
7p (2)	11.685 ± 0.106	0.329 ± 0.004	1.962	0.134 ± 0.005	0.115 ± 0.005	0.081 ± 0.003
7p (2)**	11.476 ± 0.107	0.334 ± 0.004	2.028	0.137 ± 0.004	0.117 ± 0.004	0.085 ± 0.004
13p (0.5,1)	8.695 ± 0.221	0.575 ± 0.025	5.402	0.245 ± 0.015	0.144 ± 0.011	0.165 ± 0.009
13p (0.5,2)	7.349 ± 0.109	0.592 ± 0.008	4.923	0.189 ± 0.003	0.115 ± 0.005	0.125 ± 0.007
13p (1,2)	9.952 ± 0.150	0.555 ± 0.010	3.331	0.248 ± 0.007	0.171 ± 0.008	0.116 ± 0.007
13p (1,2)**	9.823 ± 0.152	0.562 ± 0.009	3.389	0.253 ± 0.007	0.173 ± 0.009	0.119 ± 0.008
19p (0.5,1,2)	9.435 ± 0.253	0.581 ± 0.015	5.139	0.215 ± 0.008	0.146 ± 0.010	0.131 ± 0.009

*Table S2: Turbulence metrics depending on the encoding strategy for the cardiac phase corresponding to peak iTKE. Rows indicate encoding strategies, "4p (1)" refers to a 4 points encoding scheme with a single V_{enc} of $1ms^{-1}$. Integrated turbulent kinetic energy ($iTKE$), turbulence-to-noise ratio (TNR) and SSIM values of TKE and non-diagonal RST terms ($SSIM_{TKE}$, $SSIM_{R_{xy}}$, $SSIM_{R_{xz}}$, $SSIM_{R_{yz}}$) are obtained from 20 repetitions of the same acquisition. "**" refers to a scan performed by taking into consideration the additional scan efficiency of 6 and 14% for acquisitions with lowest V_{enc} = 1 and 2m/s, respectively, due to shorter TE (1.4 and 1ms vs 1.7ms for V_{enc} = 0.5m/s). For acquisitions with lowest V_{enc} = 0.5, 1 and 2m/s, TR was assumed as 5, 4.7 and 4.3ms, respectively.*

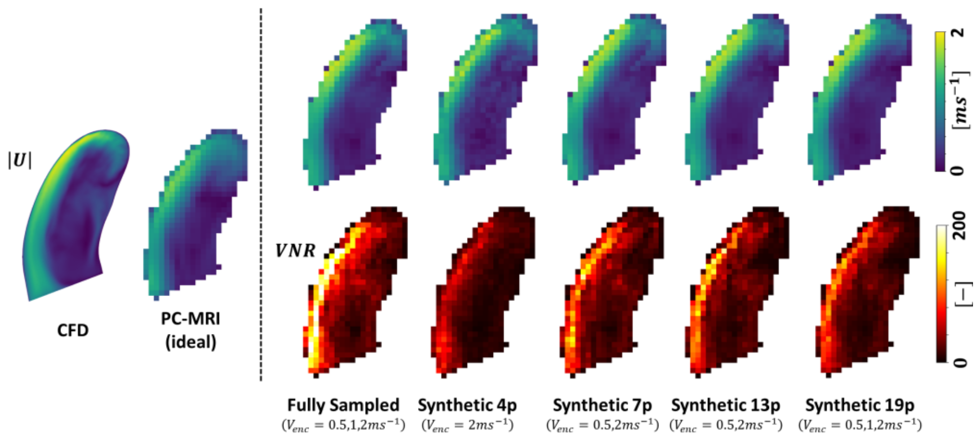

Figure S2: Peak systolic velocity magnitude maps. $|\mathbf{U}|$are the velocity magnitude maps obtained for a single acquisition. VNR represents the scan-to-scan variability of magnitude velocity maps obtained from 20 repetitions. The band-limited *reference (ideal PC-MRI) directly used averaged CFD values while all other synthetic maps were obtained by performing sequential filling of k-space and subsequent LLR reconstruction.*

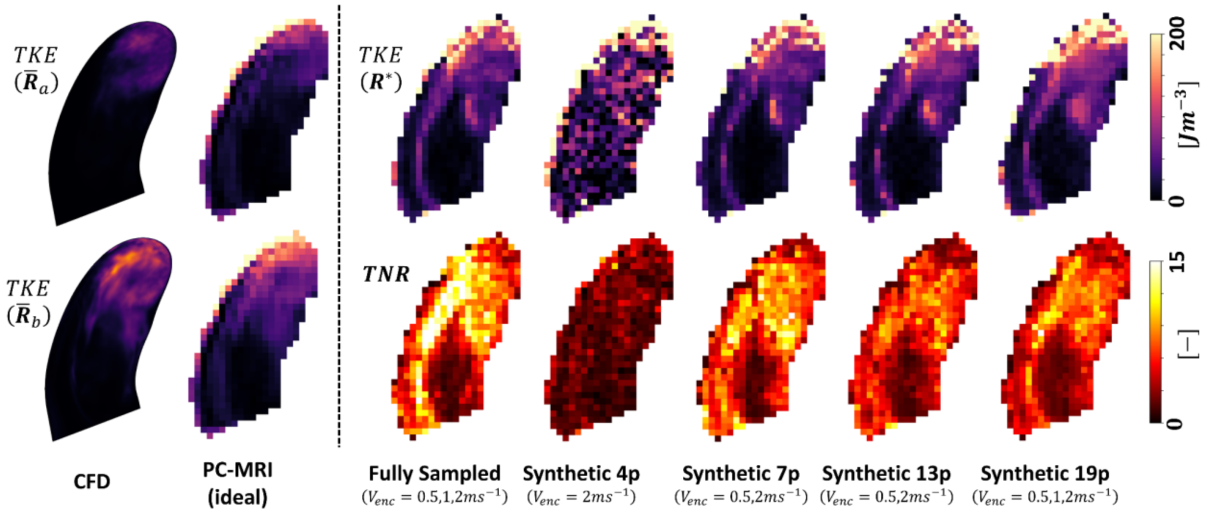

Figure S3: Peak TKE maps. TKE derived from $\boldsymbol{R}^*$ are the maps obtained for a single acquisition. TNR represents the scan-to-scan variability of TKE maps obtained from 20 repetitions. The band-limited reference (ideal PC-MRI) directly used averaged CFD values while all other synthetic maps were obtained by sequential filling of k-space and subsequent LLR reconstruction. Two averaging approaches for TKE are presented based on $\overline{\boldsymbol{R}}_a$ and $\overline{\boldsymbol{R}}_b$.

In Figure S3 it is possible to visualize the variation in TKE when using different averaging hypothesis ($\overline{\boldsymbol{R}}_a$ and $\overline{\boldsymbol{R}}_b$). The fact that MRI does not perform an arithmetic mean of TKE is clearly visible by comparing these two fields in the figure. Contrary to CFD based $\overline{\boldsymbol{R}}_b$ where purely temporal averaging of flow quantities was used, $\boldsymbol{R}^*$ obtained from sequentially filling k-space with instantaneous shots generates similar turbulence maps by using a combination of temporal and spatial averaging, supporting the observation that bulk turbulence in the aorta satisfies Taylor's hypothesis[7].

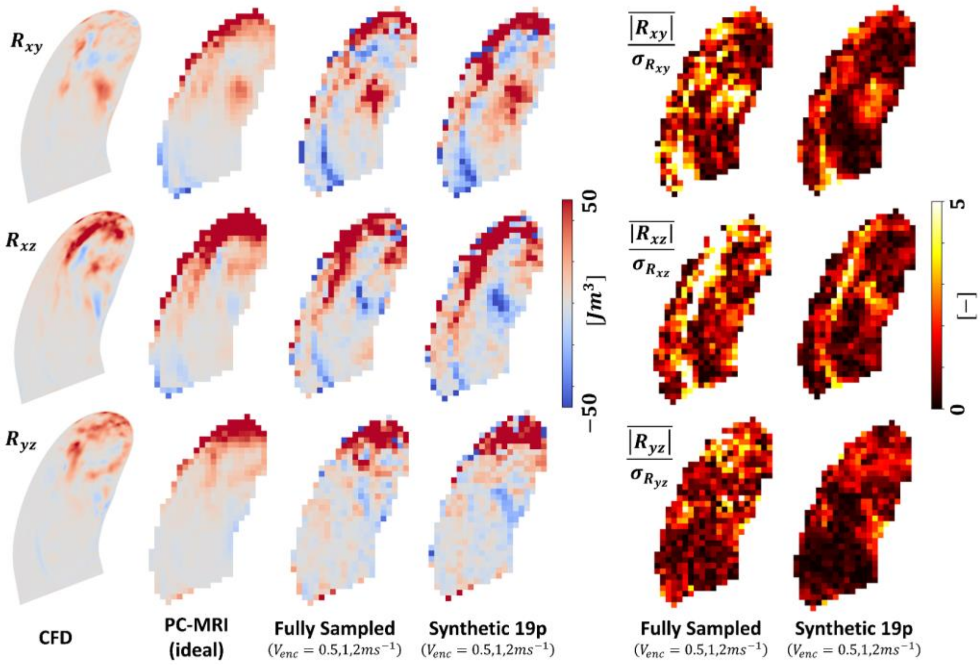

*Figure S4: Peak $\boldsymbol{R_{xy}}$, $\boldsymbol{R_{xz}}$ and $\boldsymbol{R_{yz}}$ maps. The band-limited reference (ideal PC-MRI) directly used averaged CFD values while all other synthetic maps were obtained by sequential filling of k-space and subsequent LLR reconstruction. The **Fully Sampled** and **Synthetic 19p** results were obtained for a single acquisition. An analogous metric to TNR ($\overline{|R_{ij}|} \cdot \sigma_{R_{ij}}$) adapted to the non-diagonal terms of the RST was obtained from 20 repetitions and represents their scan-to-scan variability.*

Impact of undersampling

		U_{max} $[ms^{-1}]$	iKE $[mJ]$	$iTKE$ $[mJ]$	$SSIM_U$	VNR	$SSIM_{TKI}$	TNR	$\vec{U}_{rmse}$	$\vec{\theta}_{err}$	$\nabla \cdot U$
$V_{enc} = 0.5ms^{-1}$	$\mathbf{R_u = 1.93}$ **(15min)**	2.065 ± 0.004	58.703 ± 0.101	5.411 ± 0.022	0.933 ± 0.001	65.591	0.680 ± 0.002	7.073	17.260 ± 0.107	3.844 ± 0.053	8.937 ± 0.126
	$\mathbf{R_u = 9.07}$ **(3.2min)**	2.026 ± 0.011	57.411 ± 0.094	6.274 ± 0.039	0.918 ± 0.001	42.639	0.604 ± 0.004	4.981	18.663 ± 0.148	4.145 ± 0.091	10.429 ± 0.233
	$\mathbf{R_u = 18.14}$ **(1.6min)**	1.981 ± 0.022	57.078 ± 0.203	7.609 ± 0.177	0.886 ± 0.004	22.640	0.448 ± 0.013	4.156	22.795 ± 0.298	5.077 ± 0.195	14.113 ± 0.462
$V_{enc} = 2ms^{-1}$	$\mathbf{R_u = 1.93}$ **(15min)**	2.000 ± 0.017	53.950 ± 0.083	11.334 ± 0.083	0.933 ± 0.001	28.229	0.323 ± 0.003	2.156	17.283 ± 0.143	4.271 ± 0.064	10.560 ± 0.138
	$\mathbf{R_u = 9.07}$ **(3.2min)**	1.884 ± 0.046	49.833 ± 0.102	15.059 ± 0.197	0.912 ± 0.002	19.028	0.237 ± 0.006	1.715	18.041 ± 0.167	4.445 ± 0.176	12.683 ± 0.221
	$\mathbf{R_u = 18.14}$ **(1.6min)**	1.697 ± 0.069	41.698 ± 0.444	21.743 ± 1.427	0.858 ± 0.007	9.600	0.132 ± 0.011	1.484	25.919 ± 0.649	5.920 ± 0.325	14.773 ± 0.504
Bayesian	$\mathbf{R_u = 1.93}$ **(26.3min)**	2.072 ± 0.004	58.283 ± 0.140	6.683 ± 0.046	0.939 ± 0.001	63.874	0.655 ± 0.004	6.840	15.663 ± 0.105	3.548 ± 0.054	6.876 ± 0.062
	$\mathbf{R_u = 9.07}$ **(5.6min)**	2.037 ± 0.012	56.655 ± 0.211	7.960 ± 0.076	0.919 ± 0.001	32.868	0.547 ± 0.007	4.473	16.278 ± 0.164	3.731 ± 0.089	7.808 ± 0.128
	$\mathbf{R_u = 18.14}$ **(2.8min)**	1.957 ± 0.029	50.910 ± 0.387	10.558 ± 0.308	0.868 ± 0.004	18.388	0.368 ± 0.011	3.225	21.744 ± 0.498	4.561 ± 0.191	9.983 ± 0.209

Table S3: Flow and turbulence metrics depending on the undersampling factor for two 4-point acquisitions with V_{enc}=0.5 and $2ms^{-1}$, respectively. The Bayesian combination of these measurements is also presented. Values reported correspond to the cardiac phase with peak iKE and iTKE for velocity and turbulence metrics, respectively.

Impact of breathing motion

		δ_b [−]	U_{max} [ms^{-1}]	iKE [mJ]	$iTKE$ [mJ]	$SSIM_U$	$SSIM_{TKE}$	$\vec{U}_{rmse}$	$\vec{\theta}_{err}$	$\nabla \cdot U$
$V_{enc} = 0.5ms^{-1}$	**Fully Sampled**	**0%**	2.048	58.996	5.503	0.926	0.636	17.775	4.050	9.301
		15%	2.041	56.739	5.358	0.936	0.636	16.700	3.802	8.705
		30%	2.022	54.877	5.479	0.937	0.638	16.186	3.610	8.153
		100%	1.994	57.118	6.165	0.908	0.506	19.871	4.255	10.902
	$\boldsymbol{R_u = 18.14}$ **(1.6min)**	**100%**	1.809	56.864	8.099	0.875	0.349	24.586	5.191	15.206
$V_{enc} = 2ms^{-1}$	**Fully Sampled**	**0%**	1.958	53.618	12.950	0.926	0.252	18.420	4.763	13.558
		15%	1.933	51.906	12.468	0.930	0.267	17.713	4.516	12.937
		30%	1.903	49.829	12.916	0.919	0.259	18.832	4.819	13.173
		100%	1.856	46.734	18.322	0.846	0.157	28.703	7.033	19.093
	$\boldsymbol{R_u = 18.14}$ **(1.6min)**	**100%**	1.771	34.625	26.128	0.790	0.092	34.609	7.701	15.921
Bayesian	**Fully Sampled**	**0%**	2.055	57.964	6.925	0.932	0.596	15.889	3.669	7.073
		15%	2.051	56.129	6.437	0.939	0.625	15.246	3.542	6.792
		30%	2.032	53.109	6.488	0.932	0.622	15.368	3.475	6.947
		100%	2.004	50.675	8.186	0.862	0.427	26.759	5.559	11.204
	$\boldsymbol{R_u = 18.14}$ **(2.8min)**	**100%**	1.802	42.888	12.255	0.786	0.240	34.032	6.655	14.637

Table S4: Flow and turbulence metrics depending on the undersampling factor and respiratory motion range (δ_b) for two 4-point acquisitions with $V_{enc} = 0.5$ and $2ms^{-1}$, respectively. The Bayesian combination of these measurements is also presented. A single acquisition was simulated. Values reported correspond to the cardiac phase with peak iKE and iTKE for velocity and turbulence metrics, respectively.

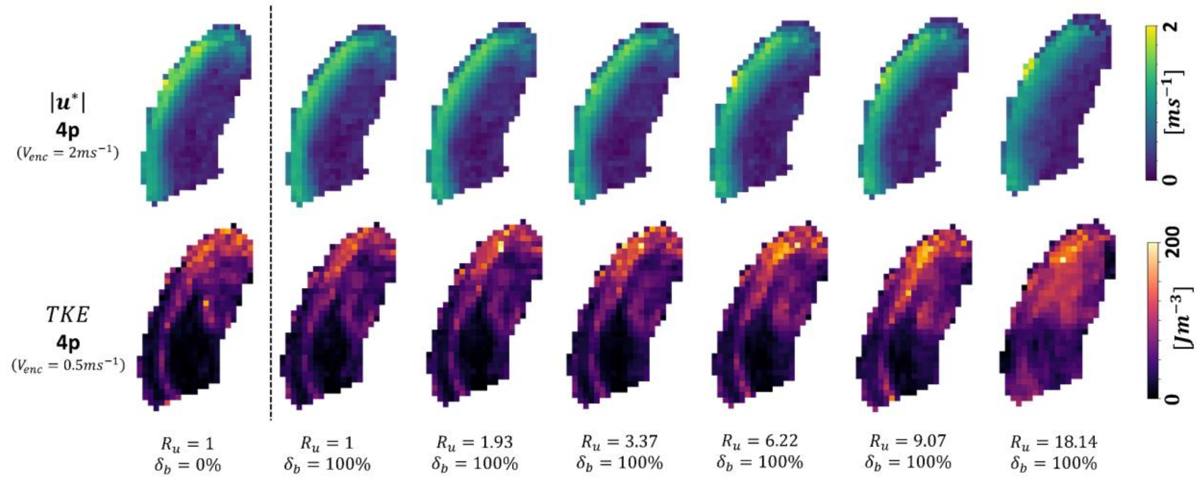

Figure S5: Peak systolic velocity magnitude and peak TKE maps. Velocity magnitude $|\boldsymbol{U}|$ was obtained from single acquisitions using different undersampling factors R_u and including respiratory motion (δ_b) for a 4-point scheme ($V_{enc} = 2ms^{-1}$). Similarly, TKE was obtained using $V_{enc} = 0.5ms^{-1}$.

Extended comments on phase unwrapping in low-$\boldsymbol{V_{enc}}$ acquisitions

All data presented in the main manuscript acquired with $V_{enc} \leq 1ms^{-1}$ was ideally unwrapped using the reference ground truth. This allowed to measure the potential of such measurements. However, unwrapping is not trivial in the case of noisy undersampled 4D flow data. Figure S6 presents the results of various unwrapping algorithms on feet-head velocity (u^*_{FH}) acquired with $V_{enc} = 0.5ms^{-1}$. For fully sampled data, the best results were obtained with a combination of NPRS and PUMA, resulting in an SSIM value for u_{FH}^* of 0.73 and 5% of residual wrapped voxels (W_ϕ). Flow rate and peak velocity error were 11.2% and -0.5%, respectively. In comparison, u_{FH}^* obtained from a fully sampled acquisition with $V_{enc} = 2ms^{-1}$ resulted in a velocity SSIM of 0.77 and flow rate and peak velocity errors of -5.2% and -5.0%, respectively. The Bayesian combination of low- and high- V_{enc} acquisitions presented a velocity SSIM of 0.76 and no error in flow rate and peak velocity estimation. In the case of undersampled data ($R_u = 18.14$), all tested unwrapping algorithms failed with more than 15% of residual unwrapped voxels. The acquisition with $V_{enc} = 2ms^{-1}$ resulted in a velocity SSIM of 0.71, and flow rate and peak velocity errors of -11.8 and 19.9%, respectively. Bayesian combination allowed to reduce flow rate and peak velocity errors to -9.7 and -6.5%, while having 5% of residual wrapped voxels. Bayesian combination inherently allows to unwrap data if the highest acquired V_{enc} is appropriate[2].

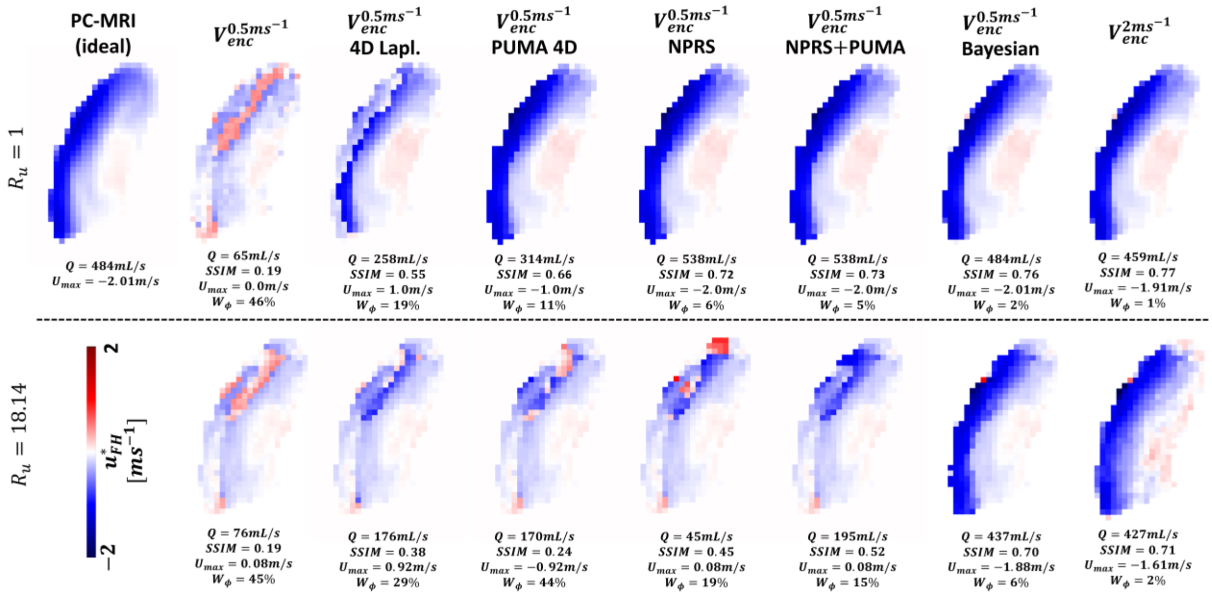

Figure S6: Results from applying Laplacian, NPRS and PUMA unwrapping to low-V_{enc} data of feet-head velocity u_{FH}^* for fully sampled and undersampled data. The reference low-V_{enc} velocity is also presented along with the high-V_{enc} velocity, and the resulting Bayesian combination. Both Q and U_{max} were computed by using exclusively u_{FH}^* and neglecting the other principal encoding directions.

Impact of SNR

In this work a fixed SNR of 20 was considered for all acquisitions. The impact of SNR is expected to shift all the relevant hemodynamic metrics without affecting the conclusions of the work. In order to visualize the impact of SNR, we showcase the results for a fully sampled 19-point scan in Figure S7 for SNR values of 10, 20, 40 and 100. Multi-V_{enc} acquisitions seem robust to changes in SNR.

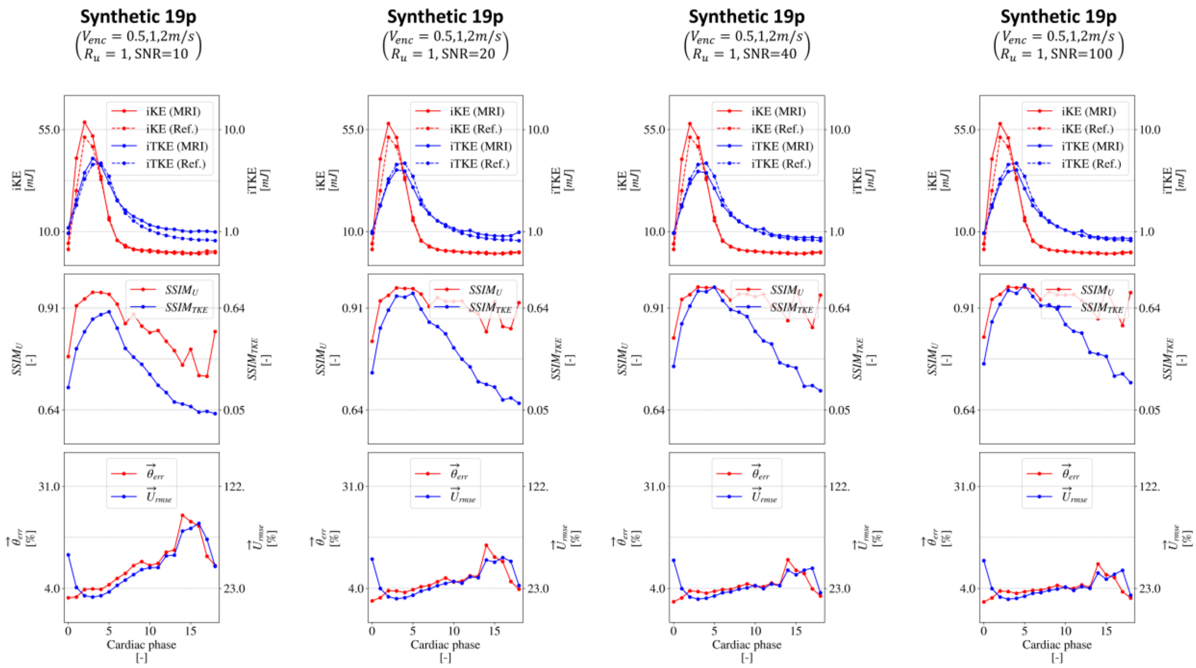

Figure S7: Impact of SNR on hemodynamic metrics of a simulated triple-V_{enc} 19-point acquisition (V_{enc}=0.5, 1 and 2m/s) with $R_u = 1$ (fully sampled), corresponding to the recommended encoding strategy for 4D-5D Flow velocity and turbulence quantification.

Recommended encoding strategy

In this work we demonstrated that low-V_{enc} acquisitions generally resulted in higher quality velocity maps due to higher VNR and lower sensitivity to undersampling (eg. underestimation of peak velocity). However, these observations are valid only if efficient phase unwrapping is available, which, as demonstrated previously, is not trivial for highly undersampled and noisy MRI data. Additionally, depending on the choice of V_{enc},TKE values are potentially underestimated. Hihg-V_{enc} acquisitions on the other hand typically are not affected by phase wrapping (if V_{enc} chosen correctly), however, they suffer from lower VNR, higher senstitivity to undersampling (eg. underestimation of peak velocity) and potential overestimation of TKE values. We observed that a dual-V_{enc} 7-point acquisition presented the best compromise, utilizing the advantages of low- and high-V_{enc}, resulting in non-aliased phase maps and turbulence maps with acceptable loss of quality. A comparison between CFD, the band-limited reference (downsampled CFD) and a dual-V_{enc} 7-point acquisition is presented in Figure S7. Both the band-limited reference and synthetic MRI data were linearly interpolated on the CFD grid before computing error metrics (this is why the error values in Figure S7 deviate from the ones reported in Tables S1, S2 and S3). Note that this deviates from the approach presented in the main manuscript, where error metrics were always computed between the various synthetic MRI data and the band-limited reference, rather than the CFD. The rationale for this choice stems from the fact that the band-limited reference is the “best” possible measurement that can be obtained from MRI, allowing us to quantify the errors in the simulated MRI data with an ideal target. An animation including all time-steps is also available (Supplemental Video 3).

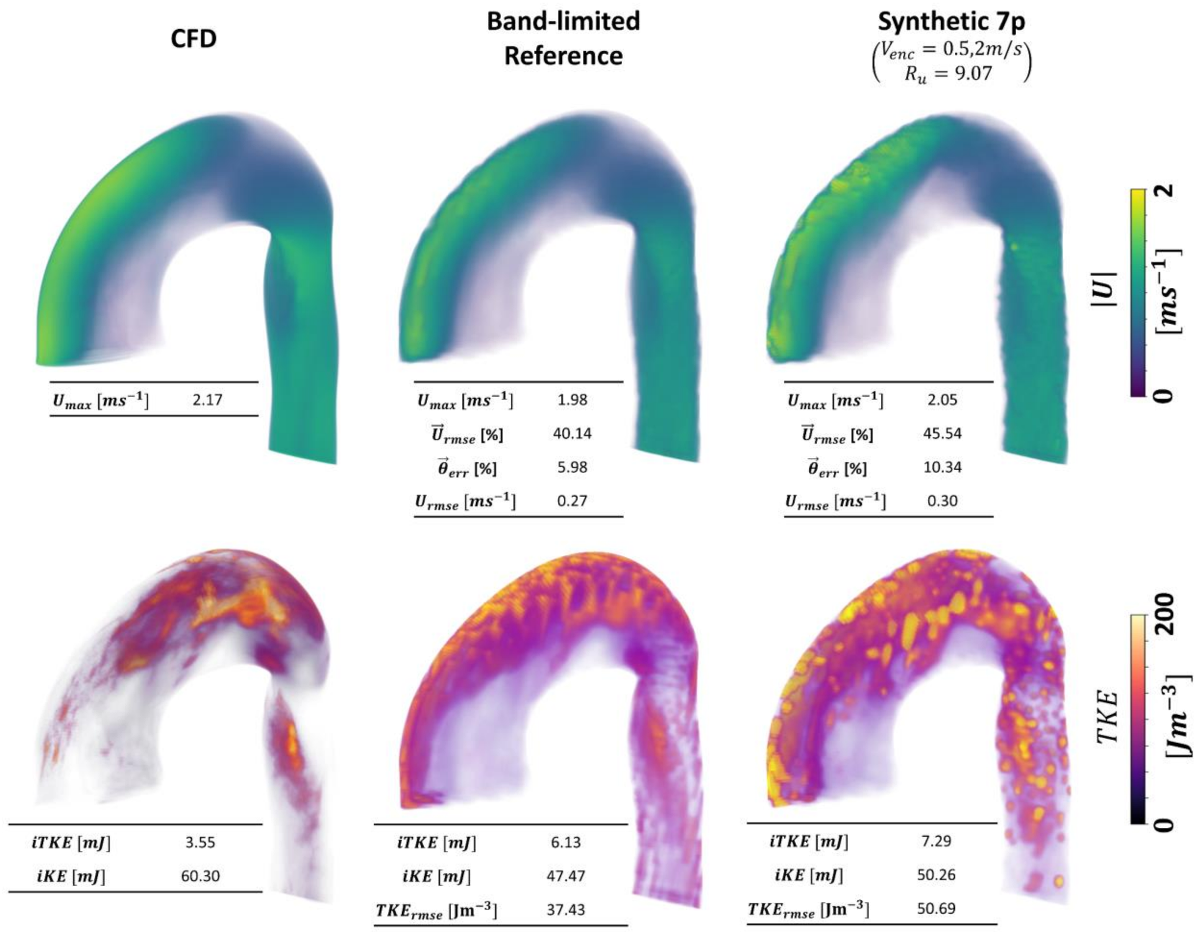

Figure S8: Velocity (at peak iKE) and TKE (at peak iTKE) maps comparison between CFD, band-limited reference (downsampled CFD) and a simulated dual-V_{enc} 7-point acquisition (V_{enc}=0.5 and 2m/s) with $R_u = 9.07$, corresponding to the recommended encoding strategy for 4D-5D Flow velocity and turbulence quantification.

Bibliography

1. Dirix, P., Buoso, S., Peper, E. S. & Kozerke, S. Synthesis of patient-specific multipoint 4D flow MRI data of turbulent aortic flow downstream of stenotic valves. *Sci. Rep.* **12**, 16004 (2022).

2. Binter, C., Knobloch, V., Manka, R., Sigfridsson, A. & Kozerke, S. Bayesian multipoint velocity encoding for concurrent flow and turbulence mapping. *Magn. Reson. Med.* **69**, 1337–1345 (2013).

3. Loecher, M., Schrauben, E., Johnson, K. M. & Wieben, O. Phase unwrapping in 4D MR flow with a 4D single-step laplacian algorithm. *J. Magn. Reson. Imaging* **43**, 833–842 (2016).

4. Herráez, M. A., Burton, D. R., Lalor, M. J. & Gdeisat, M. A. Fast two-dimensional phase-unwrapping algorithm based on sorting by reliability following a noncontinuous path. *Appl. Opt.* **41**, 7437 (2002).

5. Bioucas-Dias, J. M. & Valadao, G. Phase Unwrapping via Graph Cuts. *IEEE Trans. Image Process.* **16**, 698–709 (2007).

6. Walheim, J., Dillinger, H., Gotschy, A. & Kozerke, S. 5D Flow Tensor MRI to Efficiently Map Reynolds Stresses of Aortic Blood Flow In-Vivo. *Sci. Rep.* **9**, 1–12 (2019).

7. Taylor, G. I. The Spectrum of Turbulence. *Proc. R. Soc. London. Ser. A - Math. Phys. Sci.* **164**, 476–490 (1938).

8. Uecker, M. *et al.* ESPIRiT—an eigenvalue approach to autocalibrating parallel MRI: Where SENSE meets GRAPPA. *Magn. Reson. Med.* **71**, 990–1001 (2014).